Extinction and the optical theorem. Part I. Single particles

Matthew J. Berg,[1] Christopher M. Sorensen,[1,*] and Amitabha Chakrabarti[1]

[1]*Department of Physics, Kansas State University, Manhattan, Kansas 66506-2601, USA*
[*]*Corresponding author: sor@phys.ksu.edu*

Received November 9, 2007; revised April 10, 2008; accepted April 16, 2008; posted April 21, 2008 (Doc. ID 89499); published June 4, 2008

We study the extinction caused by a single particle and present a conceptual phase-based explanation for the related optical theorem. Simulations of the energy flow caused by a particle's presence in a collimated beam of light demonstrate how the extinction process occurs. It is shown that extinction does not necessarily cause a reduction of the energy flow along the exact forward direction. Implications regarding the measurement of the single-particle extinction cross section are discussed. This work is extended to noninteracting and interacting multiparticle groups in Part II [J. Opt. Soc. Am. A **25**, pp. 1514 (2008)]. © 2008 Optical Society of America

OCIS codes: 290.2200, 290.5850, 290.1310, 260.3160, 000.2690.

1. INTRODUCTION

Consider the situation depicted in Fig. 1. The sketch labeled (a) shows a detector with its sensitive face exposed to the energy flow of an oncoming collimated beam of light. This beam will be denoted as the incident wave, and its propagation direction as the forward direction. Now consider the sketch labeled (b). Here a particle is present, as indicated by P. The detector is assumed to be in the particle's far-field zone. With the particle present, the incident wave no longer exists due to interactions with the particle; the wave is replaced with a new wave, referred to as the total wave, that propagates and carries energy in all directions and hence accounts for the scattering of the incident beam. Energy can also be absorbed by the particle's material, and this absorption accounts for a net flow of energy into the particle's interior. The energy flows due to scattering and absorption are both figuratively illustrated in Fig. 1(b) and are associated with a reduction of the power received by the detector facing into the forward direction as shown. Extinction is the effect that describes the reduction of the power received by this detector when a particle is present.

The essence of extinction is the conservation of energy. Analogs of the above example of extinction and the related optical theorem occur in acoustical and quantum-mechanical scattering [1]. Extinction has received extensive consideration in the literature because of its importance as a fundamental aspect of electromagnetic scattering theory [2–8]. Despite this attention, however, a careful graphically based examination of how extinction occurs and the subtle details of its theoretical description, including the optical theorem, have yet to be presented. The exposition given in this article and its Part II companion will study extinction in the context of single-particle and multiparticle systems and will result in a new understanding of how extinction occurs [9]. For example, extinction is often described as the reduction of the energy flow along the forward direction due to scattering and absorption. Indeed, this is consistent with the idea behind Fig. 1 mentioned above. However, it will be shown that extinction *does not* necessarily result in a reduction of the total energy flow along the *exact* forward direction and can sometimes result in the enhancement of this flow. This forward-flow behavior is not only consistent with, but is requisite for, the conservation of energy. The measurements pertaining to Fig. 1 will be revisited, and the familiar characteristic of extinction as reducing the power received by a detector will be shown to be a consequence of the detector having a finite size.

Section 2 gives a brief review of the essential mathematics and presents the optical theorem, and Section 3 discusses some of the subtle aspects of the extinction theory. Section 4 explains how interference accounts for the redistribution of energy involved in extinction. Simulations of the energy flows caused by the interference are presented in Section 5 and show how the flows integrate to yield the extinction cross section. A connection between a particle's physical properties and its extinction cross section is discussed in Section 6. Implications regarding extinction measurements are given in Section 7, and the article ends with comments given in Section 8. The reader should note that this work and its Part II companion are not intended to provide a comprehensive review of all previous studies of extinction in the various disciplines of wave physics.

2. MATHEMATICAL BACKGROUND

The electric and magnetic fields of a monochromatic plane wave can be used to describe a collimated beam of light and are given by

$$\mathbf{E}^{inc}(\mathbf{r}) = \mathbf{E}_o^{inc} \exp(ikr\hat{\mathbf{r}} \cdot \hat{\mathbf{n}}^{inc}), \tag{1}$$

 © 2008 Optical Society of America

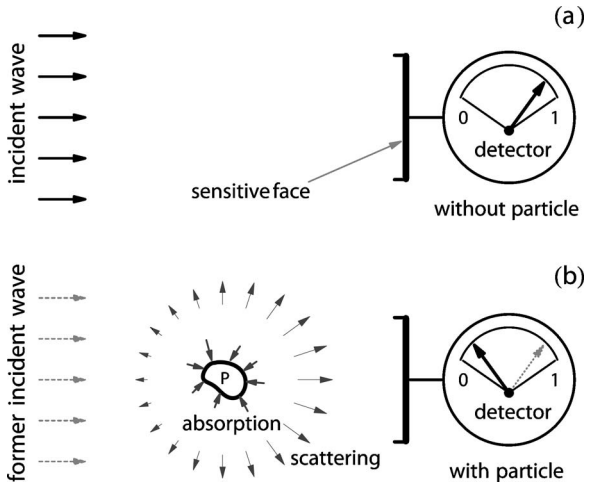

Fig. 1. Effect of extinction as described by two measurements. Sketch (a) shows a detector with its sensitive face looking into the incident beam when no particle is present. Sketch (b) shows the same situation with a particle present and labeled by P. The energy flows corresponding to the incident and scattered waves, and the flow into the particle due to absorption, are both figuratively indicated.

$$\mathbf{B}^{inc}(\mathbf{r}) = \frac{k}{\omega}\hat{\mathbf{n}}^{inc} \times \mathbf{E}^{inc}(\mathbf{r}), \tag{2}$$

respectively, where $\mathbf{E}_o^{inc}$ is a constant vector describing the amplitude and polarization of the wave (cf. [10]). Only linear polarization is considered here. The incident wave travels along the $\hat{\mathbf{n}}^{inc}$ direction with a wavenumber $k = 2\pi/\lambda$, where λ is the vacuum wavelength. The time dependence of the wave is harmonic and given by $\exp(-i\omega t)$, where ω is the angular frequency, $\omega = kc$, and c is the speed of light in vacuum. The time dependence will be suppressed for brevity.

The particle is centered on the origin of the laboratory coordinate system and is assumed to be homogeneous in composition and surrounded by vacuum. See [11–13] for generalizations to the case when the particle resides in an absorbent medium. The complex-valued refractive index of the particle is given by m. Surrounding the particle is a large imaginary spherical surface $\mathcal{S}_l$ of radius R_l centered on the origin; see Fig. 2. This surface is large enough that points on it satisfy the far-field conditions of [14]. The observation point $\mathbf{r}$ is given by the spherical polar coordinates (r, θ, ϕ) and is restricted to points on $\mathcal{S}_l$ for simplicity. The $\hat{\mathbf{n}}^{inc}$ and $-\hat{\mathbf{n}}^{inc}$ directions are referred to as the *forward* and *backward* directions, respectively. Figure 2 illustrates the scattering arrangement where the incident wave is shown with $\hat{\mathbf{n}}^{inc} = \hat{\mathbf{z}}$ and polarized parallel to the x axis.

Only the incident wave exists at $\mathbf{r}$ in the absence of the particle. With the particle present, however, a new wave exists, which can be *mathematically* decomposed into separate waves, the incident and scattered waves,

$$\mathbf{E}(\mathbf{r}) = \mathbf{E}^{inc}(\mathbf{r}) + \mathbf{E}^{sca}(\mathbf{r}), \tag{3}$$

$$\mathbf{B}(\mathbf{r}) = \mathbf{B}^{inc}(\mathbf{r}) + \mathbf{B}^{sca}(\mathbf{r}). \tag{4}$$

The particular choice of this decomposition is to facilitate a comparison between the total energy flow in the case when the particle is present and when it is absent.

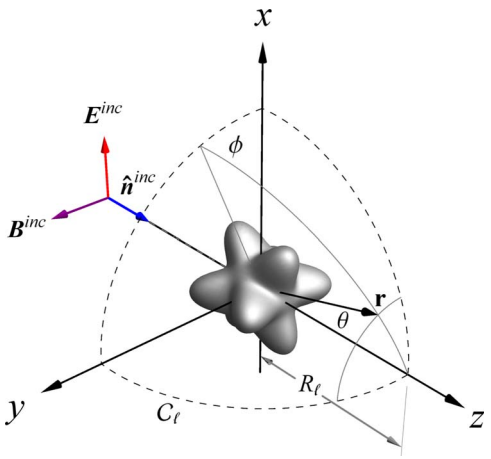

Fig. 2. (Color online) Sketch of the scattering arrangement with an arbitrarily shaped particle centered on the origin of the laboratory coordinate system. The intersection of the large spherical surface $\mathcal{S}_l$ with the x–y, y–z, and x–z planes through the origin is shown by the dashed lines. The circular contour $\mathcal{C}_l$ is defined by the intersection of $\mathcal{S}_l$ with the y–z plane as shown.

Because $\mathbf{r}$ satisfies the far-field conditions on $\mathcal{S}_l$, the scattered wave is a transverse outward-traveling spherical wave [14]. This results in a simple form for the scattered electric field,

$$\mathbf{E}^{sca}(\mathbf{r}) = \frac{\exp(ikr)}{r}\mathbf{E}_o^{sca}(\hat{\mathbf{r}}), \tag{5}$$

where $\mathbf{E}_o^{sca}$ is the so-called scattering amplitude and is independent of r. The magnetic field follows from Eq. (5) via the transverse nature of the far-field scattered wave,

$$\mathbf{B}^{sca}(\mathbf{r}) = \frac{k}{\omega}\frac{\exp(ikr)}{r}\hat{\mathbf{r}} \times \mathbf{E}_o^{sca}(\hat{\mathbf{r}}). \tag{6}$$

The scattered wave is related to the wave inside the particle. In essence, the internal wave acts as the source of the scattered wave, and the connection between the two is given by the volume integral equation (VIE) discussed in [15] and on p. 35 of [5]. The VIE can give insight into the wave-superposition origin of features of the scattered wave that can be obscured by the corresponding boundary value solutions [16]. In the VIE formalism, the far-field scattering amplitude of Eq. (5) is

$$\mathbf{E}_o^{sca}(\hat{\mathbf{r}}) = \frac{k^2}{4\pi}(m^2 - 1)(\overleftrightarrow{I} - \hat{\mathbf{r}} \otimes \hat{\mathbf{r}}) \cdot \int_V \mathbf{E}^{int}(\mathbf{r}') \times \exp(-ik\mathbf{r}' \cdot \hat{\mathbf{r}})\mathrm{d}\mathbf{r}', \tag{7}$$

where $\mathbf{E}^{int}$ is the electric field inside the particle and the integration is carried out over the particle's volume V [5,15,17]. Inspection of Eqs. (5)–(7) shows that the far-field form of the scattered fields effectively treats the particle as a point at the origin. The angular variability of the fields is described by the scattering amplitude $\mathbf{E}_o^{sca}$, which is independent of r.

The transport of energy in an electromagnetic wave is given by the Poynting vector, which in its time-averaged form is related to the fields of the wave as

$$\langle \mathbf{S}(\mathbf{r})\rangle_t = \frac{1}{2\mu_o}\,\mathrm{Re}\{\mathbf{E}(\mathbf{r}) \times [\mathbf{B}(\mathbf{r})]^*\}, \tag{8}$$

where the asterisk denotes complex conjugation and $\langle \ldots \rangle_t$ denotes time averaging [18]. The units of the Poynting vector are energy/(area × time) and hence describe an energy flux or flow. The component of $\langle \mathbf{S}\rangle_t$ directed into the sensitive face of a detector and integrated over its face is taken to represent the detector's response to the wave; see Subsection 3.6 of [15]. Note that there is some debate as to whether or not the Poynting vector gives the proper description for energy transport in a wave [19–26]. Nevertheless, the traditional interpretation of the Poynting vector is pursued here since it is well verified by measurement [26–37].

From Eqs. (3) and (4), Eq. (8) factors into three distinct terms:

$$\langle \mathbf{S}(\mathbf{r})\rangle_t = \langle \mathbf{S}^{inc}(\mathbf{r})\rangle_t + \langle \mathbf{S}^{sca}(\mathbf{r})\rangle_t + \langle \mathbf{S}^{cross}(\mathbf{r})\rangle_t, \tag{9}$$

where

$$\langle \mathbf{S}^{inc}(\mathbf{r})\rangle_t = \frac{1}{2\mu_o}\,\mathrm{Re}\{\mathbf{E}^{inc}(\mathbf{r}) \times [\mathbf{B}^{inc}(\mathbf{r})]^*\}, \tag{10}$$

$$\langle \mathbf{S}^{sca}(\mathbf{r})\rangle_t = \frac{1}{2\mu_o}\,\mathrm{Re}\{\mathbf{E}^{sca}(\mathbf{r}) \times [\mathbf{B}^{sca}(\mathbf{r})]^*\}, \tag{11}$$

$$\langle \mathbf{S}^{cross}(\mathbf{r})\rangle_t = \frac{1}{2\mu_o}\,\mathrm{Re}\{\mathbf{E}^{inc}(\mathbf{r}) \times [\mathbf{B}^{sca}(\mathbf{r})]^* + \mathbf{E}^{sca}(\mathbf{r}) \times [\mathbf{B}^{inc}(\mathbf{r})]^*\}. \tag{12}$$

Equation (10) describes the energy flow at $\mathbf{r}$ due to the incident wave, and Eq. (11) describes the flow due to the scattered wave. Notice that the cross term of Eq. (12) involves products of the fields of both the incident and scattered waves, which shows that $\langle \mathbf{S}^{cross}\rangle_t$ describes the portion of the total energy flow at $\mathbf{r}$ due to the interference of the two waves.

Electromagnetic energy will be removed from the wave if the particle's material is absorbent. This loss constitutes a net inward flow through $\mathcal{S}_l$ given by

$$W^{abs} = -\oint_{\mathcal{S}_l} \langle \mathbf{S}(\mathbf{r})\rangle_t \cdot \hat{\mathbf{r}}\,dS; \tag{13}$$

see p. 57 of [5]. The quantity W^{abs} gives the total power absorbed within the particle and is either positive or zero. Using Eq. (9), this becomes

$$W^{abs} = W^{inc} - W^{sca} + W^{cross}, \tag{14}$$

where

$$W^{inc} = -\oint_{\mathcal{S}_l} \langle \mathbf{S}^{inc}(\mathbf{r})\rangle_t \cdot \hat{\mathbf{r}}\,dS, \tag{15}$$

$$W^{sca} = \oint_{\mathcal{S}_l} \langle \mathbf{S}^{sca}(\mathbf{r})\rangle_t \cdot \hat{\mathbf{r}}\,dS, \tag{16}$$

$$W^{cross} = -\oint_{\mathcal{S}_l} \langle \mathbf{S}^{cross}(\mathbf{r})\rangle_t \cdot \hat{\mathbf{r}}\,dS. \tag{17}$$

The quantity W^{inc} gives the net power crossing $\mathcal{S}_l$ due to the incident wave, which is zero since the incident wave carries as much energy per unit time into the volume bounded by $\mathcal{S}_l$ as it carries out of the volume; see [38] and p. 57 of [5]. The quantity W^{sca} gives the net power crossing $\mathcal{S}_l$ due to the outward-traveling scattered wave and is either positive or zero. With $W^{inc}=0$, Eq. (14) now reads

$$W^{cross} = W^{sca} + W^{abs}, \tag{18}$$

which expresses the *conservation of energy* as it pertains to the energy content of the scattered wave, the interference between the incident and the scattered waves, and the energy absorbed by the particle.

To understand the meaning of W^{cross}, let the volume of space inside $\mathcal{S}_l$, including the particle, define the so-called system; see pp. 77 and 78 of [28]. Equation (18) then shows that W^{cross} is equal to the net power lost by the system due the outward-traveling scattered wave and absorption within the particle. *This net loss* is extinction, and it is a statement of the conservation of energy. Notice that the definition of extinction makes *no explicit reference to any requisite attenuation of the net energy flow along the forward direction*. This is evident from the explicit dependence in Eqs. (16) and (17) on all directions.

The scattering, absorption, and extinction cross sections C^{sca}, C^{abs}, and C^{ext} are defined from W^{sca}, W^{abs}, and W^{cross}, respectively, by normalizing the latter by the energy flux of the incident wave $I^{inc}=(\epsilon_o/\mu_o)^{1/2}|\mathbf{E}_o^{inc}|^2/2$. The optical theorem is derived by combining Eqs. (12) and (17) to give

$$W^{cross} = -\frac{1}{2\mu_o}\,\mathrm{Re}\oint_{\mathcal{S}_l} \{\mathbf{E}^{inc}(\mathbf{r}) \times [\mathbf{B}^{sca}(\mathbf{r})]^* + \mathbf{E}^{sca}(\mathbf{r}) \times [\mathbf{B}^{inc}(\mathbf{r})]^*\} \cdot \hat{\mathbf{r}}\,dS. \tag{19}$$

The plane-wave exponentials that appear in Eq. (19) through $\mathbf{E}^{inc}$ and $\mathbf{B}^{inc}$, recall Eqs. (1) and (2), can be expanded as

$$\exp(ikr\hat{\mathbf{r}} \cdot \hat{\mathbf{n}}^{inc}) = 4\pi \sum_{l=0}^{\infty} i^l j_l(kr) \sum_{m=-l}^{l} Y_{lm}^*(\hat{\mathbf{r}}) Y_{lm}(\hat{\mathbf{n}}^{inc}), \tag{20}$$

where j_l are spherical Bessel functions of the first kind and order l, and Y_{lm} are spherical harmonics; see Appendix A in [5]. By taking the limit that the observation point goes to infinity, the large-argument form of the spherical Bessel functions can be used in combination with the completeness relation for the spherical harmonics to reduce Eq. (20) to

$$\exp(ikr\hat{\mathbf{r}}\cdot\hat{\mathbf{n}}^{inc}) = 2\pi i\left[\delta(\hat{\mathbf{r}}+\hat{\mathbf{n}}^{inc})\frac{\exp(-ikr)}{kr} - \delta(\hat{\mathbf{r}}-\hat{\mathbf{n}}^{inc})\frac{\exp(ikr)}{kr}\right], \quad kr\to\infty. \tag{21}$$

Combining Eq. (19) with Eq. (21), using Eqs. (1), (2), (5), and (6), and remembering that $C^{ext}=W^{cross}/I^{inc}$ shows that the extinction cross section can be expressed as

$$C^{ext} = \frac{4\pi}{k|\mathbf{E}_o^{inc}|^2}\,\mathrm{Im}\{\mathbf{E}_o^{inc*}\cdot\mathbf{E}_o^{sca}(\hat{\mathbf{n}}^{inc})\}. \tag{22}$$

Equation (22) is the optical theorem; it relates the extinction cross section to the imaginary part of the scattering amplitude evaluated in the forward direction. An alternative way to arrive at the optical theorem from Eq. (19) is to use Jones' lemma, which utilizes the method of stationary phase to evaluate Eq. (19) in the limit that $kr\to\infty$; see Appendix 12 in [36]. Regardless of how it is derived, the optical theorem requires the limit $kr\to\infty$. This point serves as a reminder that *the theorem is only approximate in the far field and becomes strictly valid only at infinity*. In addition, the incident wave must be planar; otherwise, Eq. (22) can fail (e.g., see [40]).

3. SUBTLE NATURE OF EXTINCTION

Much of the present understanding of extinction and the physical meaning of the optical theorem traces to van de Hulst [8,39]. In that work, the removal of energy from the incident wave is claimed to be due to the interference of the incident and scattered waves in *only* the "neighborhood of the forward direction." When looking more closely, however, several questions arise. If extinction is to be regarded as the combined effect of scattering and absorption, then

- why does the optical theorem show no *apparent* account for absorption,
- why does the optical theorem involve only the forward direction when the scattered wave, upon which the theorem depends, has energy flow in all directions?

Here the answers to these questions are summarized, and the sections to follow give detail to these answers.

The dependence of extinction on a particle's absorption is hidden in the scattering amplitude $\mathbf{E}_o^{sca}$. The VIE shows that the scattering amplitude depends on the specific structure of the particle's internal electric field. The magnitude and direction of this field are affected by the absorptive properties of the particle's material.

The forward-direction dependence of the optical theorem is a result of the way that the incident and scattered waves interfere. Equations (12), (17), and (18) show that the extinction caused by the particle is given by the component of the interference energy flow that passes through $\mathcal{S}_l$ in all directions. Below it is shown that this flow alternates between inward and outward through $\mathcal{S}_l$ as a function of direction. Moreover, it is shown that the angular distribution of the alternating flow changes with distance from the particle in the far field in every direction except the exact forward direction. Because a particle's extinction cross section should be independent of the distance from the particle in the far-field zone, one can conclude that the optical theorem should then depend only on the forward direction (cf. [41,42]).

4. INTERFERENCE OF THE TWO WAVES

Consider the formulation of Eq. (17) as being the cross term between the incident and the scattered waves, i.e., the interference of these two waves [3]. Figure 3 qualitatively shows how the planar incident wave and the scattered spherical wave interfere in the far field to produce a pattern of alternating radial inward and outward flow for $\langle\mathbf{S}^{cross}\rangle_t$; see Appendix A. This happens because the relative phase between the waves changes with direction and distance from the particle and demonstrates that the waves interfere over *all directions*. This alternating flow structure is shown for points on $\mathcal{C}_l$ in Figs. 4 and 6 (below), and one can see that the inward-outward flow becomes finer with angle as the distance R_l from the particle increases. The integration of these energy flows via Eq. (28) (below), shown in Figs. 4 and 7, yields the extinction cross section C^{ext}. One can see that the energy flows in the side directions when integrated over a small angular range *nearly* yields zero due to the partial cancellation of neighboring regions of opposing radial flow. It is only when the angular range extends into the neighborhood of the forward direction that the partial cancellation be-

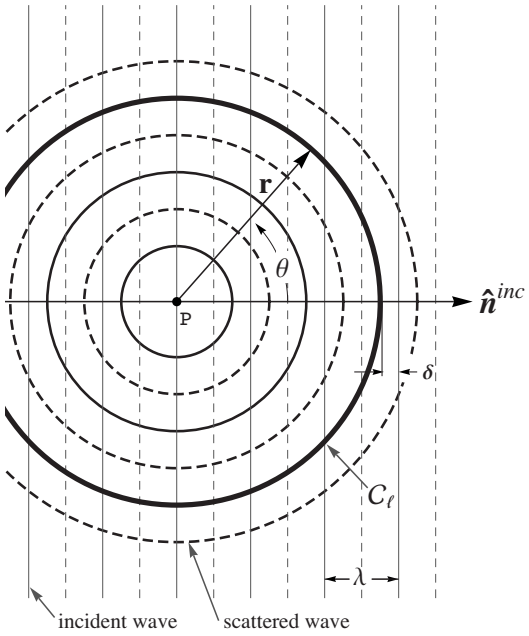

Fig. 3. Sketch showing how the incident and scattered waves interfere. The surfaces of constant phase for the two waves are drawn separated by intervals of π in phase in the plane containing the origin and perpendicular to $\mathbf{E}_o^{inc}$. The light and dark lines correspond to the surfaces for the incident and scattered waves, respectively. The relative difference in phase between the waves in the forward direction is indicated by δ. Dashed and solid lines represent maxima and minima of the waves' amplitudes, respectively. Solid–solid (dashed–solid) line intersections qualitatively indicate an outward (inward) radial component of the $\langle\mathbf{S}^{cross}\rangle_t$ energy flow; recall Eq. (24).

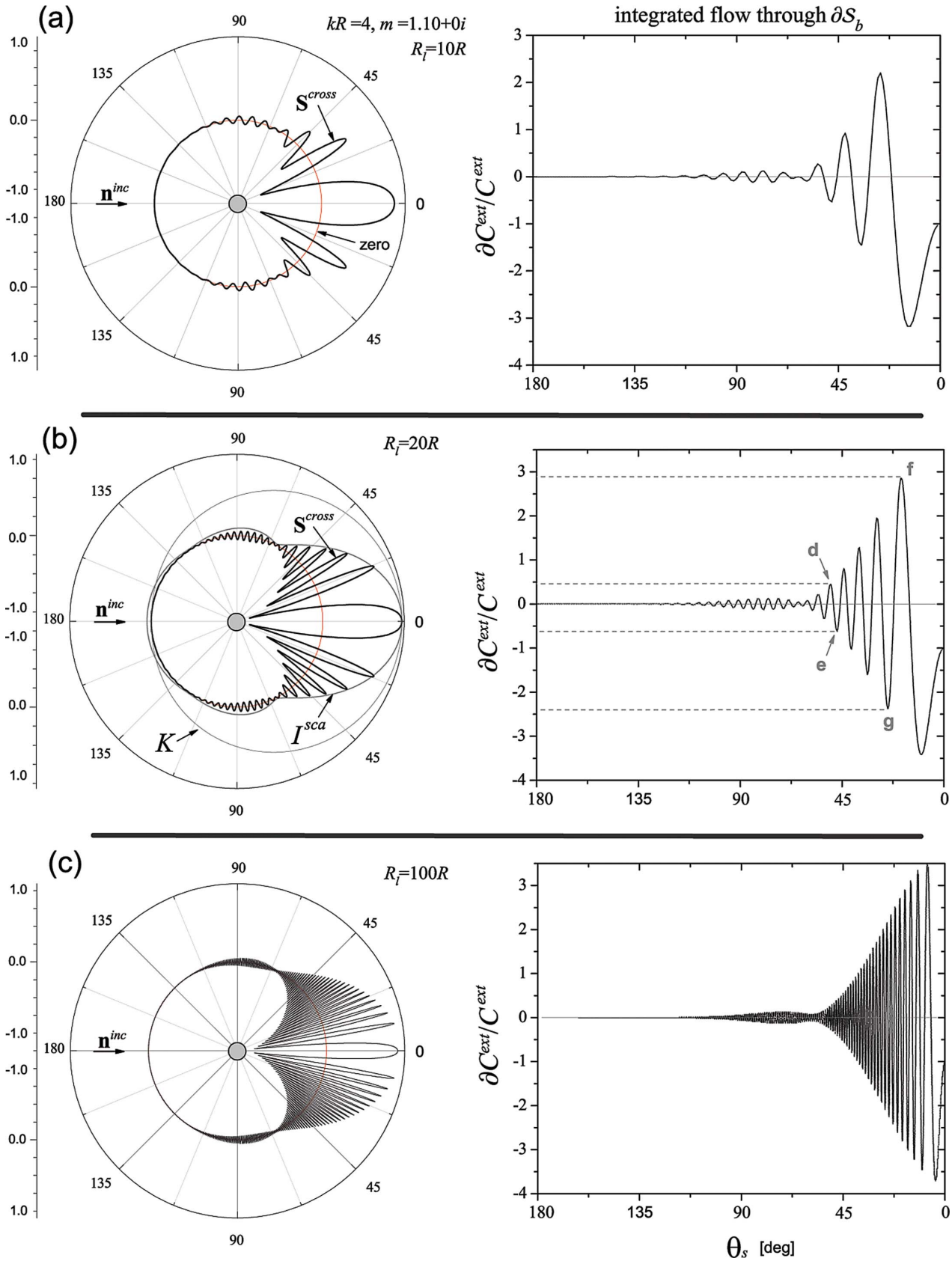

Fig. 4. (Color online) (Left column) Polar plots of $\langle \mathbf{S}^{cross} \rangle_t \cdot \hat{\mathbf{r}}$ on the $\mathcal{C}_l$ contour as a function of angle in the plane perpendicular to the polarization of the incident field. The curves are normalized to the forward direction. The particle is a sphere with $kR=4.0$ and $m=1.10+0i$. The plots labeled (a), (b), and (c) show the energy flow for increasing $\mathcal{C}_l$ contour radii $R_l=10R$, $R_l=20R$, and $R_l=100R$, respectively. Zero is indicated in polar plot (a). (Right column) Plots of the integral given by Eq. (28) normalized by C^{ext} for the contour radii indicated in the corresponding polar plots.

comes *more* incomplete, contributing to a nonzero net inward flow through $\mathcal{S}_l$ back toward the particle. Moreover, it is only after all directions, including the forward direction, are included in the integral that the full extinction cross section is obtained.

Only in the forward direction is the relative phase between the incident and the scattered waves constant in r, and it is this behavior of the relative phase and the planar surfaces of constant phase of the incident wave that give the optical theorem its unidirectional character. One can see the independence of the relative phase between these waves in the forward direction by comparing the exponential terms in Eqs. (1), (2), (5), and (6). The independence of $\mathbf{E}_o^{sca}$ on r is what makes the relative phase constant in the forward direction and is a direct consequence of the far-field form of the scattered wave.

This graphical-based reasoning can be made more rigorous. In the process, the role of absorption in extinction is revealed and a connection between the extinction cross section and a particle's physical characteristics is obtained. In the following, the observation point is restricted to the circular contour $\mathcal{C}_l$. For the arrangement shown in Fig. 2, this contour resides in the $y-z$ plane as indicated and is defined by the intersection of this plane with $\mathcal{S}_l$. Consequently,

$$\hat{\mathbf{r}} \cdot \mathbf{E}_o^{inc} = \hat{\mathbf{r}} \cdot \mathbf{E}_o^{sca} = 0, \quad \mathbf{r} \in \mathcal{C}_l, \tag{23}$$

and using Eqs. (1), (2), (5), (6), and (12), the radial component of the interference term in the total Poynting vector can be expressed as

$$\langle \mathbf{S}^{cross}(R_l\hat{\mathbf{r}})\rangle_t \cdot \hat{\mathbf{r}} = \frac{c_o}{R_l} K(\hat{\mathbf{r}}) \mathrm{Re}\{f_o(\hat{\mathbf{r}}) \exp[ikR_l(1 - \hat{\mathbf{r}} \cdot \hat{\mathbf{n}}^{inc})]\},$$

$$\mathbf{r} \in \mathcal{C}_l, \tag{24}$$

where $c_o = (\epsilon_o/\mu_o)^{1/2}$ and

$$K(\hat{\mathbf{r}}) = 1 + \hat{\mathbf{r}} \cdot \hat{\mathbf{n}}^{inc}, \tag{25}$$

and

$$f_o(\hat{\mathbf{r}}) = \mathbf{E}_o^{inc*} \cdot \mathbf{E}_o^{sca}(\hat{\mathbf{r}}). \tag{26}$$

Note that $\langle \mathbf{S}^{cross}\rangle_t$ has components along the $\hat{\boldsymbol{\theta}}$ and $\hat{\boldsymbol{\phi}}$ directions also, but it is only the $\hat{\mathbf{r}}$ component that carries energy away from (or toward) the particle and hence is of interest here. The term K in Eq. (24) is the so-called obliquity factor, which vanishes in the backward direction $-\hat{\mathbf{n}}^{inc}$ and originates from the counterpropagation of the two waves in that direction.

The significance of the two terms inside the Re{…} filter in Eq. (24) requires some care to describe. The first term, f_o, is a complex-valued function of angle that accounts for the variation in magnitude and phase of the scattered electric field. By comparing Eqs. (7) and (26), one can see that f_o is independent of r and receives its angular functionality from the phase factor $\exp(-ik\mathbf{r}' \cdot \hat{\mathbf{r}})$ in the VIE [cf. Eq. (7)]. This shows that f_o describes the influence of the particle's physical properties, like size and shape, on the interference energy flow. By comparing the exponential factors appearing in Eqs. (1) and (5), one finds that the factor $\exp[ikR_l(1-\hat{\mathbf{r}}\cdot\hat{\mathbf{n}}^{inc})]$ in Eq. (24) accounts for the angular dependence of the *relative* difference in phase between the incident and the scattered waves. This term has no dependence on the physical properties of the particle and hence accounts for the features of the interference energy flow that are a consequence of the form of the waves in the far-field zone.

The angular structure of $\langle \mathbf{S}^{cross}\rangle_t$ shown in Fig. 4 can now be explained. As $\mathbf{r}$ advances along the $\mathcal{C}_l$ contour, the term $\exp[ikR_l(1-\hat{\mathbf{r}}\cdot\hat{\mathbf{n}}^{inc})]$ oscillates, causing the radial component of $\langle \mathbf{S}^{cross}\rangle_t$ to alternate from being directed away from to toward the particle. The function f_o is an angular envelope bounding this energy flow. Moreover, if one considers the intensity of the scattered wave, which is given by Eq. (11) as $I^{sca}(\hat{\mathbf{r}}) = r^2\langle \mathbf{S}^{sca}(\mathbf{r})\rangle_t \cdot \hat{\mathbf{r}}$, then Eqs. (5), (6), and (23) show that

$$I^{sca}(\hat{\mathbf{r}}) = \frac{c_o}{2} \mathbf{E}_o^{sca}(\hat{\mathbf{r}}) \cdot [\mathbf{E}_o^{sca}(\hat{\mathbf{r}})]^*, \tag{27}$$

which involves the same angular functionality as f_o [cf. Eq. (26)]. Figure 4(b) shows I^{sca} and K superimposed on the interference flow. Both curves are normalized to the forward direction, and one can see the influence that I^{sca} and K have on the angular shape of the overall envelope bounding the flow.

5. EXAMPLES OF THE ENERGY FLOW CAUSED BY A SINGLE SPHERICAL PARTICLE

Simulations of spherical particles are examined below to illustrate how $\langle \mathbf{S}^{cross}\rangle_t$ describes extinction and integrates over $\mathcal{S}_l$ to yield C^{ext}. Both the scattered fields and the extinction cross section for the particle are found from the Mie solution to the Maxwell equations following Section 4 of [7].

First consider a small spherical particle with size parameter $kR = 4.0$ and refractive index $m = 1.10 + 0i$, where R is the sphere radius. The propagation and polarization directions of the incident wave are taken to be $\hat{\mathbf{n}}^{inc} = \hat{\mathbf{z}}$ and $\mathbf{E}_o^{inc} = \hat{\mathbf{x}}$, respectively. The polar plots in Figs. 4(a)–4(c) show the radial component of the $\langle \mathbf{S}^{cross}\rangle_t$ energy flow along the $\mathcal{C}_l$ contour for successively larger values of R_l. To see how this energy flow integrates over $\mathcal{S}_l$ to yield C^{ext} through Eq. (17), consider the integral

$$\partial C^{ext}(\theta_s) = \frac{1}{I^{inc}} \int_{\partial \mathcal{S}_b} \langle \mathbf{S}^{cross}(\mathbf{r})\rangle_t \cdot \hat{\mathbf{r}} \mathrm{d}S. \tag{28}$$

The symbol ∂ is not intended to represent a derivative. The open surface $\partial\mathcal{S}_b$ in Eq. (28) is the part of the large (closed) spherical surface $\mathcal{S}_l$ that extends from $\theta = \pi$, the backward direction, to $\theta = \theta_s$; see Fig. 5(a). When $\theta_s = \pi$, $\partial\mathcal{S}_b$ disappears, and when $\theta_s = 0$, $\partial\mathcal{S}_b = \mathcal{S}_l$. Notice that there is a sign difference between Eqs. (17) and (28) so that

$$C^{ext} = -\partial C^{ext}(0). \tag{29}$$

Shown in the right-hand column of Fig. 4 are plots of the integral $\partial C^{ext}/C^{ext}$ as θ_s varies from π down to zero. The value of C^{ext} is calculated directly from the Mie series to verify that the integral in Eq. (28) does indeed yield the correct cross section when $\theta_s = 0$.

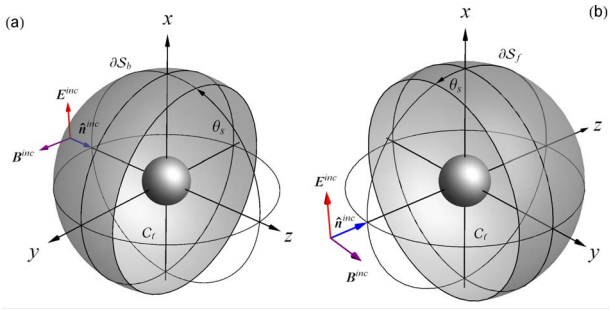

Fig. 5. (Color online) Partial surfaces $\partial\mathcal{S}_b$ and $\partial\mathcal{S}_f$ surrounding the spherical particles used to generate the plots of $\partial C^{ext}/C^{ext}$ in Figs. 4 and 7 via Eq. (28). In sketch (a), the surface begins in the backward direction at $\theta=\pi$ and extends to $\theta=\theta_s$. In sketch (b), the surface begins in the forward direction at $\theta=0$ and extends to $\theta=\theta_s$.

In the polar plot in Fig. 4(a), $R_l=10R$ and the $\langle\mathbf{S}^{cross}\rangle_t$ energy flow is seen to alternate from radially outward to inward, as expected from Eq. (24). The zero line is labeled in this plot. Examination of the corresponding plot of $\partial C^{ext}/C^{ext}$ shows that it oscillates about zero until around $\theta_s=0$, where $\partial C^{ext}(0)/C^{ext}=-1$; recall Eq. (29). This negative value at $\theta_s=0$, where the partial surface $\partial\mathcal{S}_b$ becomes complete, coinciding with $\mathcal{S}_l$, indicates that $\langle\mathbf{S}^{cross}\rangle_t$ *carries a net inward flow of energy through* $\mathcal{S}_l$. This *net* inward flow *is* the extinction and demonstrates why the negative sign appears in front of the integral in Eq. (17), ensuring that $C^{ext}\geqslant 0$.

Figures 4(b) and 4(c) show the energy flow for increasing $\mathcal{C}_l$ contour radii $R_l=20R$ and $R_l=100R$, respectively. These polar plots demonstrate that the flow becomes finer with increasing R_l but remains unchanged in the forward and backward directions, as expected from Fig. 3. One can also clearly see the diminishment of the flow near the backward direction.

Now consider the two pairs of peaks labeled d, e and f, g. Comparison of these peaks shows that each successive peak is slightly greater in magnitude than the peak preceding it in θ_s. Moreover, the difference in magnitude between successive peaks increases as θ_s approaches zero. Consequently, the partial cancellation of angular regions of opposing energy flow becomes less complete nearer to the forward direction. In the limit that $kR_l\to\infty$, the peaks would be spaced infinitesimally close together in angle and would be infinite in number but would still occur in opposing-flow peak pairs. In this case the contribution to the extinction cross section would still originate from the (infinitesimally) incomplete cancellation of neighboring angular regions of opposing flow. This limiting behavior of the energy flow is the physical significance behind the method of stationary phase as it is used to derive the optical theorem (cf. [36]).

The plots of $\langle\mathbf{S}^{cross}\rangle_t$ in Fig. 4 share a key common feature. *The flow alternates radially more rapidly with angle as* R_l *increases, but the direction of the flow along* $\hat{\mathbf{n}}^{inc}$ *remains unchanged*. Inspection of these plots shows that when the integral in Eq. (17) adds up this alternating flow over $\mathcal{S}_l$, it will add together regions of opposing flow of *nearly* equal magnitude in the side scattering directions. These regions of opposing flow will partially cancel each other's contribution to the integral. The plots of $\partial C^{ext}/C^{ext}$ in Fig. 4 show the cancellation between adjacent regions of opposing flow becoming less complete closer to the forward direction. *This is why extinction has the appearance of being a forward angle effect*.

To examine the affect of absorption on extinction, Fig. 6 shows polar plots like Fig. 4, but for a larger sphere with increasing values of $\mathrm{Im}(m)$. The plots show the same qualitative behavior as the nonabsorbent spheres, demonstrating that absorption does not remove the radially alternating character of the interference energy flow. Consequently, extinction is still achieved via the same interference mechanisms described above.

Notice that between Figs. 4 and 6, the increased size and refractive index of the particles causes the direction of energy flow along $\hat{\mathbf{n}}^{inc}$ to change. This unexpected behavior is explained by evaluating Eq. (24) in the $\hat{\mathbf{n}}^{inc}$ direction with the substitution of Eqs. (32) and (33) below, giving

$$\langle\mathbf{S}^{cross}(r\hat{\mathbf{n}}^{inc})\rangle_t\cdot\hat{\mathbf{n}}^{inc}=2A\frac{c_o}{r}\cos\sigma. \tag{30}$$

Because both C^{ext} and A are necessarily nonnegative, Eq. (34) below shows that σ above is bounded in $[0,\pi)$. Equation (30) then reveals that the energy flow *should* alternate in direction along $\hat{\mathbf{n}}^{inc}$ as σ varies with changes in the physical properties of the particle through Eq. (33).

Figure 7 shows the integral of Eq. (28) for the absorbent spheres in Fig. 6. Except for a different perspective, the integral is taken over the partial surface $\partial\mathcal{S}_f$ shown in Fig. 5(b). This surface begins in the forward direction at $\theta=0$ and extends to $\theta=\theta_s$. Indicated in the legend of Fig. 7 are the extinction cross sections for each of the three spheres as calculated directly from the Mie series. Also indicated on each curve is the value of ∂C^{ext} when the partial surface $\partial\mathcal{S}_f$ closes at $\theta_s=\pi$ and coincides with $\mathcal{S}_l$. The use of $\partial\mathcal{S}_f$ instead of $\partial\mathcal{S}_b$ demonstrates the expected result that it does not matter from which direction, forward or backward, the alternating energy flow is integrated. The curves clearly show that the dominant contribution to the cross section occurs near the forward direction as stated by van de Hulst [8]. Comparing Figs. 6 and 7 demonstrates that *the direction of the energy flow along* $\hat{\mathbf{n}}^{inc}$ *can be either toward or away from the particle and the correct extinction cross section is still obtained upon integration of the flow over all directions*.

6. CONNECTION TO THE PARTICLE'S PHYSICAL PROPERTIES

Using the VIE for the scattering amplitude, it is possible to demonstrate how the physical properties of the particle, i.e., its size, shape, and refractive index, affect the extinction cross section. From Eq. (7), the amplitude profile f_o appearing as the argument of the $\mathrm{Im}\{\ldots\}$ filter in the optical theorem [Eq. (22)] is

$$\mathbf{E}_o^{inc_*}\cdot\mathbf{E}_o^{sca}(\hat{\mathbf{n}}^{inc})=\frac{k^2}{4\pi}(m^2-1)\int_V\mathbf{E}_o^{inc_*}\cdot\mathbf{E}^{int}(\mathbf{r}')\times\exp(-ik\mathbf{r}'\cdot\hat{\mathbf{n}}^{inc})d\mathbf{r}', \tag{31}$$

where use has been made of the transverse character of

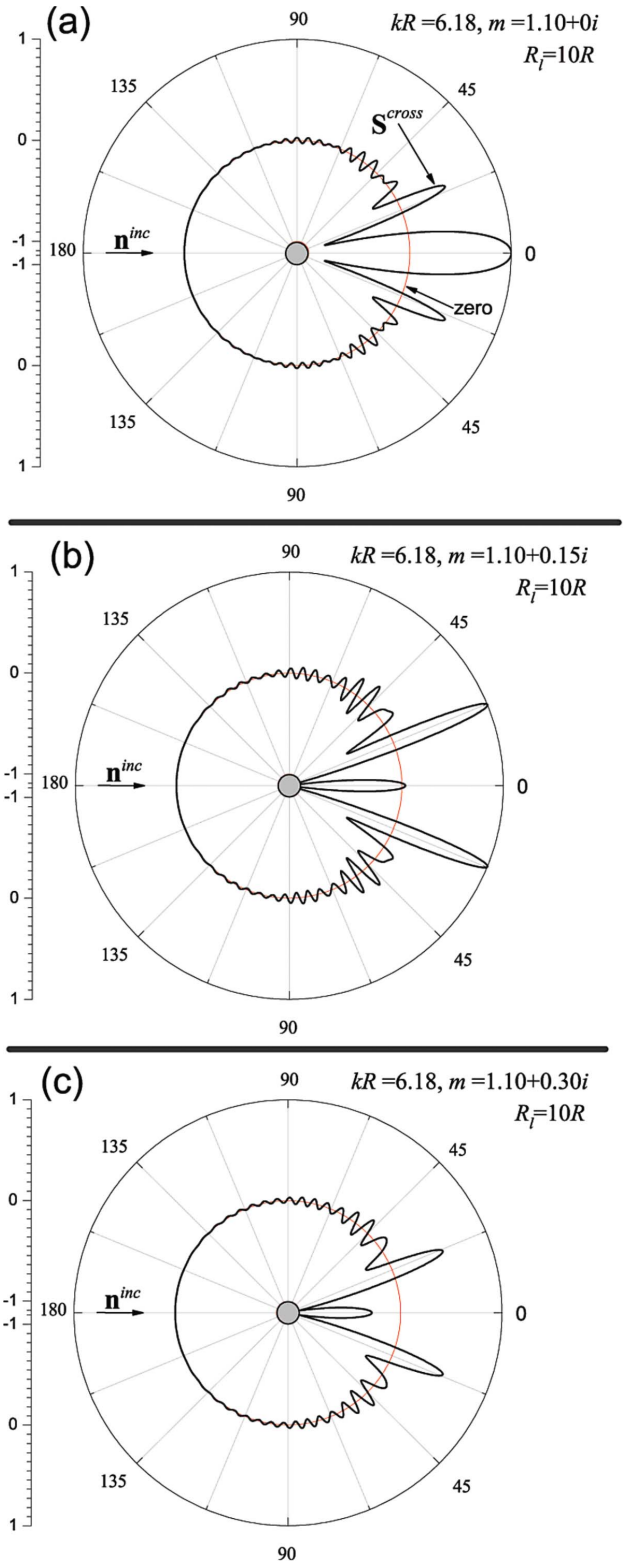

Fig. 6. (Color online) Polar plots of $\langle \mathbf{S}^{cross} \rangle_t \cdot \hat{\mathbf{r}}$ on the C_l contour like Fig. 4 except for spheres with varying degrees of absorption. The size parameter of the particles is $kR=6.18$, and their refractive index varies from $m=1.10+0i$ in (a), to $m=1.10+0.15i$ in (b), to $m=1.10+0.30i$ in (c). The contour radius is $R_l=10R$.

the far-field scattered wave and the relation $\mathbf{E}_o^{inc*} \cdot (\hat{\mathbf{n}}^{inc} \otimes \hat{\mathbf{n}}^{inc}) \cdot \mathbf{E}^{int} = 0$. Using Eq. (31), one can define an amplitude and phase factor as

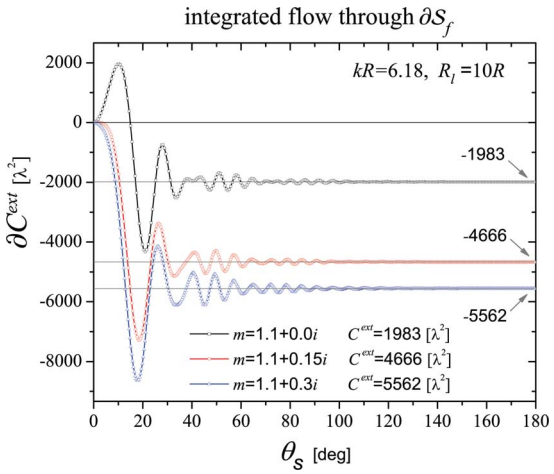

Fig. 7. (Color online) Plots of the integral $\partial C^{ext}/C^{ext}$ of Eq. (28) for the interference energy flow due to the spheres in Fig. 6. The partial surface ∂S_f used to generate the curves extends from $\theta=0$ to $\theta=\theta_s$ and is shown in Fig. 5(b). The size of the surface is $R_l=20R$. The values for C^{ext} in the legend are calculated directly from the Mie series for comparison to the values shown on the curves at $\theta_s=\pi$.

$$A = |\mathbf{E}_o^{inc*} \cdot \mathbf{E}_o^{sca}(\hat{\mathbf{n}}^{inc})|, \tag{32}$$

and

$$\sigma = \tan^{-1}\left\{ \frac{\mathrm{Im}[\mathbf{E}_o^{inc*} \cdot \mathbf{E}_o^{sca}(\hat{\mathbf{n}}^{inc})]}{\mathrm{Re}[\mathbf{E}_o^{inc*} \cdot \mathbf{E}_o^{sca}(\hat{\mathbf{n}}^{inc})]} \right\}, \tag{33}$$

respectively, which when combined with Eq. (22) gives

$$C^{ext} = \frac{4\pi}{k|\mathbf{E}_o^{inc}|^2} A \sin\sigma. \tag{34}$$

This result is essentially equivalent to the form appearing in [8,39].

To see how the optical theorem relates the particle's physical properties to C^{ext} through Eq. (34), first suppose that the particle is absorbent. This would mean that $\mathrm{Im}(m) \geq 0$. Referring to Eq. (33) shows that this can cause σ to increase, and thus increase C^{ext}, as compared to an identical particle without absorption. This provides a connection between the particle's absorption and its influence on the extinction cross section; but there is more to this. The appearance of absorption in a particle causes its internal field to change as compared to its nonabsorbent counterpart. With absorption, the field magnitude decays with distance into the particle, and near its inner surface, the field becomes directed more tangential to the surface; see pp. 352–356 of [27]. This then provides an indirect connection and could counteract the enhancement in C^{ext} due to $\mathrm{Im}(m)$, as mentioned above. Similarly, the size of the particle, its shape, and its orientation if it is nonspherical, all directly affect the structure of the internal field and hence the value of the integral appearing in Eqs. (32) and (33), leading to the cross section through Eq. (34).

7. IMPLICATIONS REGARDING THE MEASUREMENT OF THE EXTINCTION CROSS SECTION FOR A SINGLE PARTICLE

Perhaps the most intuitive way to measure the extinction cross section is as the difference in the response of a detector facing into the forward direction with and without a particle present. This measurement is illustrated in Fig. 1 and is discussed in detail in [8]. The essential idea behind the measurement is that the total power that reaches the detector's face is reduced by the presence of the particle and that the reduction is proportional to C^{ext}. The following examines this measurement within the context of the energy flow plots presented in Figs. 4 and 7.

The response of a detector will be given by the component of the *total* energy flow $\langle \mathbf{S} \rangle_t$ directed into and integrated over its sensitive face. When the particle is present in the beam, $\langle \mathbf{S} \rangle_t$ is given by Eq. (9) and contains three contributions: $\langle \mathbf{S}^{inc} \rangle_t$, $\langle \mathbf{S}^{sca} \rangle_t$, and $\langle \mathbf{S}^{cross} \rangle_t$. Each of these contributions has different dependencies on the distance r between the particle and the detector. From Eqs. (5), (6), and (10)–(12), one can see that $\langle \mathbf{S}^{inc} \rangle_t$ is independent of r, $\langle \mathbf{S}^{sca} \rangle_t$ decays as r^{-2}, and $\langle \mathbf{S}^{cross} \rangle_t$ decays as r^{-1}. Consequently, in the far-field zone the total energy flow $\langle \mathbf{S} \rangle_t$ will be dominated by the contributions from $\langle \mathbf{S}^{inc} \rangle_t$ and $\langle \mathbf{S}^{cross} \rangle_t$.

Now consider Fig. 8, which shows the same situation as in Fig. 1(b) except with the three contributions to $\langle \mathbf{S} \rangle_t$ explicitly indicated along with their relative magnitude. Here the detector is the partial spherical surface $\partial \mathcal{S}_f$ shown in Fig. 5(b) with an angular size given by θ_s. The detector is located in the particle's far-field zone, and its size is taken to be much greater than the particle's geometric projection into the forward direction but small enough as not to exceed the width w of the incident beam.

The component of the total energy flow due to $\langle \mathbf{S}^{inc} \rangle_t$ is approximately constant over the detector's face and is directed into it. This means that the detector receives, in part, an amount of power equal to the product of the flux of the incident wave I^{inc} and the area of its face. Added to this power is the contribution due to $\langle \mathbf{S}^{cross} \rangle_t$, which is given by ∂C^{ext} in Eq. (28). The magnitude of the contribution from $\langle \mathbf{S}^{inc} \rangle_t$ is always greater than that of $\langle \mathbf{S}^{cross} \rangle_t$ in the far-field zone due to the latter's inverse dependence on r. Consequently, the detector always encounters a *net* flow of energy directed *into* its face and hence always registers a positive power. However, the contribution to this net power due to $\langle \mathbf{S}^{cross} \rangle_t$ can either subtract from or add

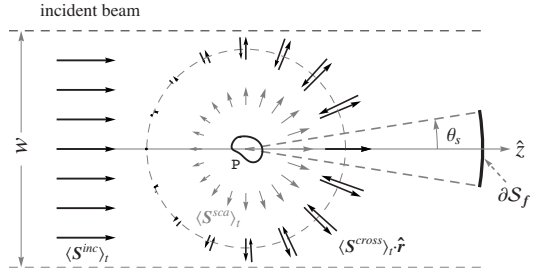

Fig. 8. This sketch shows the same situation as in Fig. 1(b) except with the three contributions to the total energy flow qualitatively indicated. Here the detector is the partial surface $\partial \mathcal{S}_f$ shown in Fig. 5(b) and the solid angle subtended by the detector is given by θ_s.

to the contribution due to $\langle \mathbf{S}^{inc} \rangle_t$ depending on the detector's angular size. This is evident from Fig. 7, which shows that ∂C^{ext} can be either positive or negative depending on the value of θ_s. *It is only after a sufficiently large solid angle of the total energy flow is accommodated by the detector that the contribution from* $\langle \mathbf{S}^{cross} \rangle_t$ *reduces the power received by the detector by an amount corresponding to* C^{ext}. For the three particles considered in Fig. 7, the detector's angular size would have to be $\theta_s \geqslant 60^\circ$ in order to include enough of the forward interference energy flow to measure C^{ext} to within a few percent error.

Refer again to the plot in Fig. 7 and suppose that the angular size of the detector depicted in Fig. 8 is $\theta_s = 15^\circ$. Inspection of this plot shows that the contribution to the net power received by the detector due to $\langle \mathbf{S}^{cross} \rangle_t$ would be negative for the $m = 1.10 + 0.15i$ and $m = 1.10 + 0.30i$ particles, whereas it would be positive for the $m = 1.10 + 0i$ particle. This means that the power received by the detector when the $m = 1.10 + 0.15i$ or $m = 1.10 + 0.30i$ particle is present will be less than the power received by the detector in the particle's absence, as expected. However, if the $m = 1.10 + 0i$ is present, the power received by the detector is *greater* than when the particle is absent. Recalling that the curves in Fig. 7 are calculated from Fig. 6, one can see that the origin of this unexpected behavior is that the $\langle \mathbf{S}^{cross} \rangle_t$ energy flow near the forward direction is oriented away from the particle in Fig. 6(a), whereas it is oriented toward the particle in Figs. 6(b) and 6(c). Note that energy conservation is not violated in this example, since the detector is not collecting all 4π steradians of the total energy flow; recall Eqs. (14)–(18).

8. COMMENTS

Although only uniform spherical particles are considered in the simulations in this work, the conclusions regarding the interference-based energy flow mechanism behind extinction apply to any arbitrary particle. Inhomogeneous particles require a generalization of the VIE to include variations in the refractive index, and nonspherical particles require an account of their orientation with respect to the incident wave.

An important result of this work is to show that extinction does not necessarily result in the reduction of the power received by a detector facing into the forward direction when a particle is present. Whether or not the detector in the far-field zone receives a reduced amount of power depends on the detector's angular size. The magnitude of the total energy flow along the exact forward direction can either be reduced or enhanced as compared with that of the incident wave.

Finally, the reader familiar with the use of Beer's law to measure the extinction coefficient of a dilute colloid or aerosol may be troubled that the measurements discussed in Section 7 require a detector with an angular size exceeding 60°. Such measurements on dilute colloids and aerosols are known to yield the correct extinction coefficient for far smaller detector solid angles. Part II of this work will generalize the single-particle analysis presented above to multiparticle groups and demonstrate that the presence of multiple particles causes the dominant contribution to the group's extinction cross section to

reside within a narrower angular region around the forward direction; this will resolve the apparent inconsistency with Beer's law [9].

APPENDIX A

Confusion can arise when trying to identify the surfaces of constant phase of the far-field scattered wave. Clearly, the term $\exp(ikr)/r$ in Eq. (5) is constant in both magnitude and phase on spherical surfaces centered on the origin. One can see from Eq. (7) that $\mathbf{E}_o^{sca}$ will, in general, vary in magnitude and phase on these same spherical surfaces. One could take the surfaces of constant phase of the wave to be spheres and then regard $\mathbf{E}_o^{sca}$ as a complex-valued angular weighting function that varies over these surfaces. Alternatively, one could use Euler's formula to express the right-hand side of Eq. (5) or (6) as $[A(\hat{\mathbf{r}})/r]\exp[i\phi(\hat{\mathbf{r}})]$, where both A and ϕ are real-valued functions of direction and are independent of r. In this case the surfaces of constant $\phi(\hat{\mathbf{r}})$ will not in general be spheres. It ultimately does not matter how one describes the geometry of the surfaces of constant phase; the crucial feature of the form of the far-field wave is that the scattering amplitude $\mathbf{E}_o^{sca}$ be independent of r.

ACKNOWLEDGMENTS

The authors are grateful for the suggestions and encouragement given by Michael Mishchenko and O. Larry Weaver, the discussions with Anatoli Borovoi, and the useful comments of the two reviewers. This work was supported by the NASA Graduate Student Researchers Program.

REFERENCES

1. R. G. Newton, "Optical theorem and beyond," Am. J. Phys. **44**, 639–642 (1976).
2. M. I. Mishchenko, "The electromagnetic optical theorem revisited," J. Quant. Spectrosc. Radiat. Transf. **101**, 404–410 (2006).
3. A. G. Borovoi, "Multiple scattering of short waves," in *Light Scattering Reviews: Single and Multiple Scattering*, A. A. Kokhanovsky, ed. (Springer, 2006), pp. 181–252.
4. P. S. Carney, J. C. Schotland, and E. Wolf, "Generalized optical theorem for reflection, transmission, and extinction of power for scalar fields," Phys. Rev. E **70**, 036611 (2004).
5. M. I. Mishchenko, L. D. Travis, and A. A. Lacis, *Scattering, Absorption, and Emission of Light by Small Particles* (Cambridge U. Press, 2002), p. 3 and Secs. 2.5 and 2.8; freely available in pdf format at http://www.giss.nasa.gov/~crmim/books.html.
6. R. G. Newton, *Scattering Theory of Waves and Particles* (Dover, 2002).
7. C. F. Bohren and D. R. Huffman, *Absorption and Scattering of Light by Small Particles* (Wiley, 1983), Secs. 3.4 and 11.
8. H. C. van de Hulst, *Light Scattering by Small Particles* (Dover, 1981), Secs. 4.21, 4.22, and 4.3.
9. M. J. Berg, C. M. Sorensen, and A. Chakrabarti, "Extinction and the optical theorem. Part II. Multiple particles," J. Opt. Soc. Am. A **25**, 1514–1520 (2008).
10. A. E. Siegman, *Lasers* (University Science Books, 1986), Sec. 17.
11. M. I. Mishchenko, "Electromagnetic scattering by a fixed finite object embedded in an absorbing medium," Opt. Express **15**, 13188–13202 (2007).
12. G. Videen and W. Sun, "Yet another look at light scattering from particles in absorbing media," Appl. Opt. **42**, 6724–6727 (2003).
13. P. Chýlek, "Light scattering by small particles in an absorbing medium," J. Opt. Soc. Am. **67**, 561–563 (1977).
14. M. I. Mishchenko, "Far-field approximation in electromagnetic scattering," J. Quant. Spectrosc. Radiat. Transf. **100**, 268–276 (2006).
15. M. I. Mishchenko, L. D. Travis, and A. A. Lacis, *Multiple Scattering of Light by Particles: Radiative Transfer and Coherent Backscattering* (Cambridge U. Press, 2006), Sec. 3.1.
16. M. J. Berg, C. M. Sorensen, and A. Chakrabarti, "Reflection symmetry of a sphere's internal field and its consequences on scattering: a microphysical approach," J. Opt. Soc. Am. A **25**, 98–107 (2008).
17. C. T. Tai, *Dyadic Green Functions in Electromagnetic Theory* (IEEE, 1994), pp. 6–11.
18. J. A. Stratton, *Electromagnetic Theory* (McGraw-Hill, 1941), Sec. 2.19.
19. H. A. Lorentz, *The Theory of Electrons* (Dover, 2003), pp. 25–26.
20. C. Jeffries, "A new conservation law for electrodynamics," J. Soc. Ind. Appl. Math. **34**, 386–405 (1992).
21. C. Jeffries, "A response to commentary by F. N. H. Robinson," J. Soc. Ind. Appl. Math. **36**, 638–641 (1992).
22. R. H. Romer, "Alternatives to the Poynting vector for describing the flow of electromagnetic energy," Am. J. Phys. **50**, 1166–1168 (1982).
23. C. S. Lai, "Alternative choice for energy flow vector of the electromagnetic field," Am. J. Phys. **49**, 841–843 (1981).
24. D. F. Nelson, "Generalizing the Poynting vector," Phys. Rev. Lett. **76**, 4713–4716 (1996).
25. G. J. J. Rikken and B. A. van Tiggelen, "Direction of optical energy flow in a transverse magnetic field," Phys. Rev. Lett. **78**, 847–850 (1997).
26. U. Backhaus and K. Schäfer, "On the uniqueness of the vector for energy flow density in electromagnetic fields," Am. J. Phys. **54**, 279–280 (1986).
27. J. D. Jackson, *Classical Electrodynamics* (Wiley, 1999), pp. 258–262.
28. E. J. Rothwell and M. J. Cloud, *Electromagnetics* (CRC, 2001), pp. 85–88.
29. W. Gough, "Poynting in the wrong direction?" Eur. J. Phys. **3**, 83–87 (1982).
30. I. Campos and J. L. Jiménez, "About Poynting's theorem," Eur. J. Phys. **13**, 117–121 (1992).
31. P. C. Peters, "Objections to an alternate energy flow vector," Am. J. Phys. **50**, 1165–1168 (1982).
32. A. Chubykalo, A. Espinoza, and R. Tzonchev, "Experimental test of the compatibility of the definitions of the electromagnetic energy density and the Poynting vector," Eur. Phys. J. D **31**, 113–120 (2004).
33. F. N. H. Robinson, "Poynting's vector: comments on a recent paper by Clark Jeffries," J. Soc. Ind. Appl. Math. **36**, 633–637 (1994).
34. M. Nakajima, "Physical meaning of the Poynting vector and the resolution of paradoxes (basic concept 2)," Electron. Commun. Jpn., Part 2: Electron. **82**, 56–69 (1999).
35. J. D. Jackson, "How an antenna launches its input power into radiation: the pattern of the Poynting vector at and near an antenna," Am. J. Phys. **74**, 280–288 (2006).
36. M. Born and E. Wolf, *Principles of Optics* (Cambridge U. Press, 1999), pp. 7–10.
37. D. H. Kobe, "Energy flux for the electromagnetic field and gauge invariance," Am. J. Phys. **50**, 1162–1164 (1982).
38. A. Doicu, T. Wriedt, and Y. A. Eremin, *Light Scattering by Systems of Particles* (Springer, 2006), p. 50.
39. H. C. van de Hulst, "On the attenuation of plane waves by obstacles of arbitrary size and form," Physica (Amsterdam) **15**, 740–746 (1949).
40. J. A. Lock, J. T. Hodges, and G. Gouesbet, "Failure of the optical theorem for Gaussian-beam scattering by a spherical particle," J. Opt. Soc. Am. A **12**, 2708–2715 (1995).
41. C.-T. Tai, "Backward scattering theorem applying to a perfectly conducting sphere," J. Electromagn. Waves Appl. **16**, 597–609 (2002).
42. J. A. Grzesik, "A note on the backward scattering theorem," Prog. Electromagn. Res. **40**, 255–269 (2003).